AGU PUBLICATIONS

JGR

Journal of Geophysical Research: Space Physics

RESEARCH ARTICLE
10.1002/2016JA023482

Special Section:
Major Results From the MAVEN Mission to Mars

He bulge revealed: He and CO_2 diurnal and seasonal variations in the upper atmosphere of Mars as detected by MAVEN NGIMS

M. K. Elrod[1,2], S. Bougher[3], J. Bell[4], P. R. Mahaffy[1], M. Benna[1,5], S. Stone[6], R. Yelle[6], and B. Jakosky[7]

[1]NASA Goddard Space Flight Center, Greenbelt, Maryland, USA, [2]CRESST, University of Maryland, College Park, Maryland, USA, [3]Climate and Space Sciences and Engineering Department, University of Michigan, Ann Arbor, Michigan, USA, [4]National Institute of Aerospace, Hampton, Virginia, USA, [5]CRESST, University of Maryland, Baltimore County, Baltimore, Maryland, USA, [6]Lunar and Planetary Laboratory and Department of Planetary Sciences, University of Arizona, Tucson, Arizona, USA, [7]Laboratory for Atmospheric and Space Physics, University of Colorado Boulder, Boulder, Colorado, USA

Key Points:
- Data using MAVEN NGIMS for 1 Martian year reveal diurnal and seasonal variations in He and CO_2 indicating a changing He bulge in upper atmosphere
- Observed He bulge is found to agree preliminarily with M-GITM modeling efforts
- He bulge found at Mars is similar to those found at Earth and Venus

Correspondence to:
M. K. Elrod,
meredith.k.elrod@nasa.gov

Citation:
Elrod, M. K., S. Bougher, J. Bell, P. R. Mahaffy, M. Benna, S. Stone, R. Yelle, and B. Jakosky (2017), He bulge revealed: He and CO_2 diurnal and seasonal variations in the upper atmosphere of Mars as detected by MAVEN NGIMS, *J. Geophys. Res. Space Physics*, *122*, 2564–2573, doi:10.1002/2016JA023482.

Received 16 SEP 2016
Accepted 26 JAN 2017
Accepted article online 31 JAN 2017
Published online 23 FEB 2017

Abstract Analysis of the Neutral Gas and Ion Mass Spectrometer (NGIMS) on the Mars Atmosphere Volatiles and EvolutioN (MAVEN) spacecraft closed source data from all orbits with good pointing revealed an enhanced Helium [He] density on the nightside orbits and a depressed He density on the dayside by about a factor of 10–20. He was also found to be larger in the polar regions than in the equatorial regions. The northern polar winter nightside He bulge was approximately twice that of the northern polar summer nightside bulge. The first 6 weeks of the MAVEN prime mission had periapsis at high latitudes on the nightside during northern winter, followed by the midlatitudes on the dayside moving to low latitudes on the nightside returning to the high latitudes during northern summer. In this study we examined the NGIMS data not only in the different latitudes but sorted by solar longitude (Ls) in order to separate the diurnal or local solar time (LST) effects from the seasonal effects. The Mars Global Ionosphere-Thermosphere Model (M-GITM) has predicted the formation of a He bulge in the upper atmosphere of Mars on the nightside early morning hours (Ls = 2–5 h) with more He collecting around the poles. Taking a slice at constant altitude across all orbits indicates corresponding variations in He and CO_2 with respect to LST and Ls and a diurnal and seasonal dependence.

1. Introduction

Helium [He] in the terrestrial atmospheres of Venus, Earth, and Mars can be used as a tracer for vertical advection and wind currents in the upper atmosphere. Vertical advection and neutral winds are very difficult to directly measure and have mainly been modeled.

The Mars Atmosphere and Volatiles EvolutioN (MAVEN) [*Jakosky et al.*, 2014] spacecraft has been in orbit around Mars since September 2014 observing the upper atmosphere. The Neutral Gas Ion Mass Spectrometer (NGIMS) [*Mahaffy et al.*, 2014] began operations in late October 2014 with observations during the encounter of Comet Siding Spring and regular science operations beginning in November 2014. Within the prime mission (November 2014 to December 2015) MAVEN performed four deep dips, and in the extended mission (January 2016 to August 2016) the spacecraft performed two more deep dips where the spacecraft passed lower into the atmosphere than its normal operations, closer to ~120 km.

During its normal operations MAVEN periapsis altitude is generally around 150 km allowing it to measure the traditional exobase region near 200 km. MAVEN began the science mission in the northern polar region remaining above 45°N from solar longitude (Ls) 216–262 and 88–150, was in the equatorial region (between latitude 45°N and −45°S) from Ls = 289–339, 50–100, and 150–189, and dipped into the southern polar region (latitude < 45°S) from Ls 331–50. This has provided the opportunity to examine the northern polar region at winter and summer, the southern polar region during equinox, and the equatorial region through equinox and near the two solstices. By sorting the data into northern and southern polar regions and equatorial regions, we are better able to examine diurnal and possible seasonal effects.

For this study, we are focusing mainly on the diurnal and seasonal variations of the He density measured at 4 dalton (Da) and CO_2 secured by using measurements at 44 Da or at fragment or isotope masses in those cases where the 44 signal saturated the detector. The 44 Da signal can also be attenuated to enable this measurement at lower altitudes. Predictions from the three-dimensional Mars Global Ionosphere-Thermosphere

Model (M-GITM) [*Bougher et al*., 2015b; *Bell et al*., 2015; *Bougher et al*., 1990] indicate that He densities should be enhanced on the nightside (local solar time (LST) = 2–5 h) and around the poles, in contrast to lower densities on the dayside or around the equator. At Ls = 90 and 270 (solstices), the He bulge is expected to be highest on the nightside southern and northern poles, respectively. At Ls = 0 and 180 (equinoxes), the He bulge is expected to be highest near dawn at midlatitudes. He peaks in the equatorial region are expected to occur near equinox as the bulge is shifting from one pole to the other [*Bell et al*., 2015; *Kasprzak et al*., 1993].

He bulges have been detected at Earth, Venus, and now confirmed at Mars. Earlier observations of the Venus atmosphere by the Pioneer Venus mission indicate that there is a significant day/night variation in the He densities [*Niemann et al*., 1980]. Observations of He, prior to MAVEN, in the Martian atmosphere were limited to the dayside and, thus, the day/night variations were theorized based on the observations made at Venus [*Krasnopolsky*, 2002; *Krasnopolsky et al*., 1994; *Krasnopolsky and Gladstone*, 2005; *Bougher et al*., 1986; *Bougher and Roble*, 2003]. Previous observations of He in the Martian atmosphere conducted by the Viking lander upon entry [*Kasprzak et al*., 1993; *Kasprzak*, 1969; *Neir and McElroy*, 1977]. MAVEN is the first orbiter at Mars with the capabilities necessary to observe the He atmosphere down to ~120 km. At Earth, He was found to be dependent on the local vertical advection and molecular diffusion in the upper atmosphere [*Liu et al*., 2014; *Sutton et al*., 2015]. The upward summer winds depress the He density, while the downward winter winds greatly increase the He density in the upper atmosphere above the homeopause. This driving force causes the He to collect in the upper latitudes creating a He bulge.

1.1. Methods: NGIMS Data

NGIMS is a quadropole mass spectrometer (qms) designed to measure neutral gas from 2 to 150 Da. It has the ability to attenuate the sensor, twice, when the detector becomes saturated. The maximum counts per second (cps) that the detector is able to read before saturation is ~10^7. We have the capability of detuning the focusing lenses such that the signal will be attenuated by a factor of ~10 and a factor of ~100 at each detuning. This allows the qms to detect densities to much higher concentrations particularly for Ar and CO_2 which will typically saturate the detector at our nominal attenuation as primary constituents of the upper atmosphere will reach densities ~10^{10}–10^{11} part/cm^3 for CO_2. The high concentration of Ar, CO_2, and the subspecies CO and O in the atmosphere, m44, m16, m28, and m40, amongst a few others, will consistently saturate the unattenuated detector. Therefore, it is necessary to correct the saturated masses with the attenuated signals. While CO_2 and Ar will saturate and need to be corrected, He never saturates the detector and thus is uncorrected other than for background counts. In this paper we focus on background subtracted and corrected masses 4 and 44. In addition, NGIMS alternates between a closed source mode and an open source mode. On a normal science run, the closed source neutral mode is run every orbit, for consistency and calibration. Because we can directly calibrate the sensitivity of the closed source, we use this mode to compute the abundances for the nonreactive species Ar, He, CO_2, N_2, and CO. The open source mode will alternate between neutral beaming mode and filaments off for ion mode [*Mahaffy et al*., 2015]. For this study, since we are using only He and CO_2, we are able to use the closed source data, which are run every orbit.

We used data from 18 October 2014, obtained during the encounter with Comet Siding Spring, through 4 August 2016, MAVEN NGIMS level 2 version 06 revision 02 neutral data. In order to reduce instrumentation effects, all data are restricted to the inbound portion of the pass. While He is nonreactive to the interior of the instrument, CO_2 reacts with the interior of the instrument and has a much higher background on the outbound. This made for inconsistent He/CO_2 ratios between inbound versus outbound due to an instrumental effect rather than an atmospheric effect. Note that all NGIMS data are in IAU coordinates and altitude is measured to the Martian Aeroid not the surface.

We binned the data in the following manner: altitude (alt) in 1 km steps from 150 km to 350 km, local solar time (LST) in 1 h steps from 0 h to 24 h, and latitude in 6° steps from −90° to 90°. In addition, we took a slice of the data at a constant altitude of 200 km in order to compare the variations in the He density over time, latitude, and LST by removing altitude variations. We chose to use LST for our analysis because it is easier to demonstrate dawn versus dusk asymmetry in the CO_2 and He densities. The M-GITM model predicts the He bulge will collect at the poles and around LST = 2–5 h. Figure 1 depicts the He density over all altitudes versus LST (a) and slices around the northern pole LAT > 45°N (b), southern pole LAT < −45° (c), and equatorial region between LAT 45° and −45° (d). In each of these panels the peak He density occurs in the region of LST = 2–5 h with a secondary peak around LST = 22–24 h.

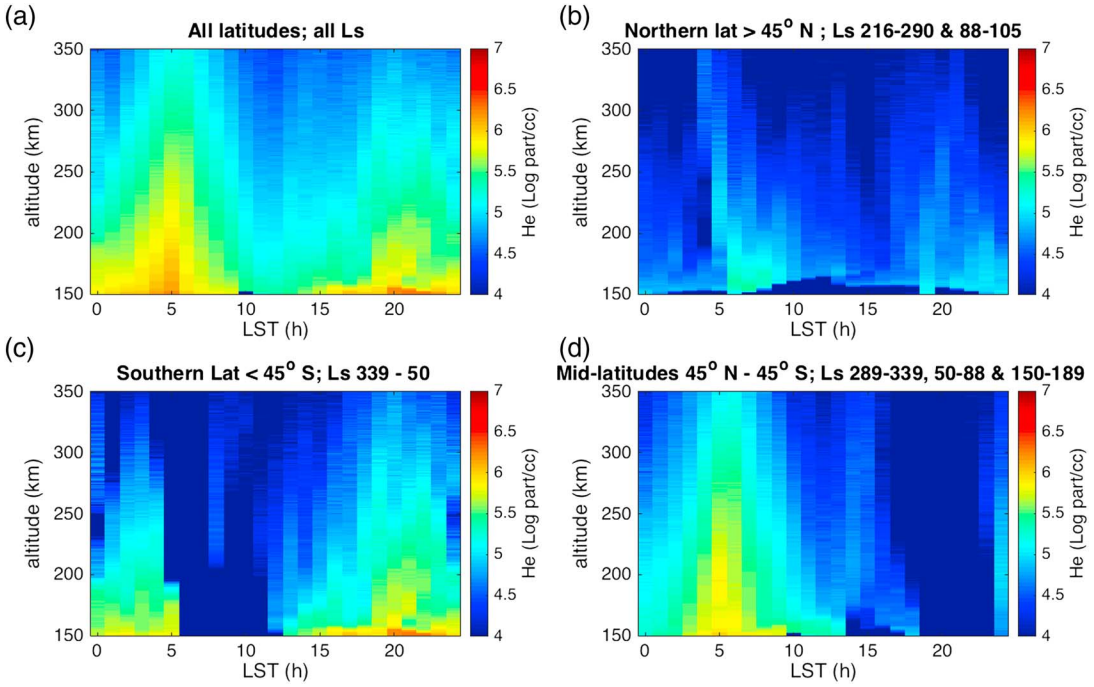

Figure 1. (a) LST versus ALT (LST versus altitude (alt)) for all orbits from 150 km to 350 km in 1 km steps from 0 to 24 h in 1 h steps. (b) Selecting data with latitudes above 45° focusing on the He collecting around the northern polar region. (c) Selecting data with latitudes below −45° focusing on the southern polar region. (d) All remaining data between latitudes 45° and −45° creating an equatorial band, less likely to be affected by seasonal effects, but still highly affected by LST. All four panels indicate a peak around 2–5 h LST and a secondary peak around 20–21 h. The peak at 5 h is approximately 20 times higher than the data at 12 h, while the peak at 20 h is approximately 10 times higher.

In Figure 2 we took a single inbound vertical profile slice from two different orbits in order to compare the CO_2 and He from dayside to nightside. Dayside orbit 931 (CO_2: red connected circles; He: green no line crosses) shows a higher CO_2 scale height, and higher CO_2 abundance above 150 km. Conversely, the He abundance is barely above noise level, and it is difficult to determine a scale height. Nightside orbit 3209 (CO_2: blue connected crosses; He: magenta no line circles) shows just the opposite. CO_2 has a much lower scale height with abundances lower below 150 km, while He abundances are much higher, well above any possible background noise levels. The He scale height is still difficult to determine, but the profile is less noisy than the dayside counterpart. With CO_2 being the most abundant species in the atmosphere we compared He/CO_2 in order to be able to track the He bulge over seasonal expansion/contraction of the atmosphere. Figure 4 tracks the ratio of He/CO_2 with LST and demonstrates how the diurnal effects on the bulge enhance the He densities particularly at the poles.

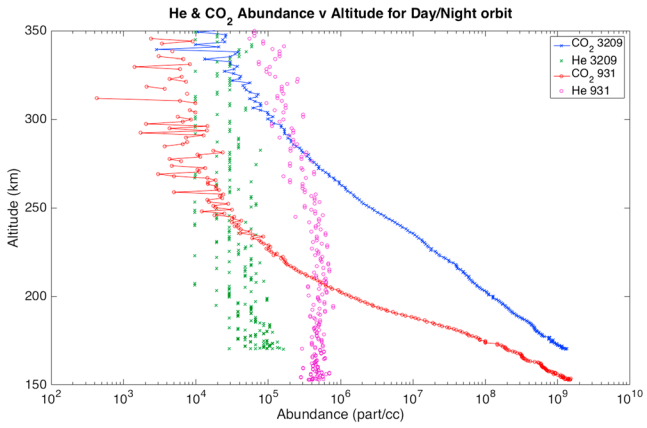

Figure 2. One nightside (931) and one dayside (3209) altitude versus abundance profile from 150 to 350 km for CO_2 and He on the inbound portion of the orbit. Crosses are for dayside orbit 3209 LST = 13–14 h, blue connected for CO_2 and green no line for He. Open circles are for nightside orbit 931 LST = 4–6 h, red connected for CO_2 and magenta no line for He.

MAVEN has been in orbit around Mars for nearly one Martian year starting at Ls = 216 to Ls = 198. MAVEN started the mission in the northern polar region from Ls = 216–262, during northern winter. The second pass in

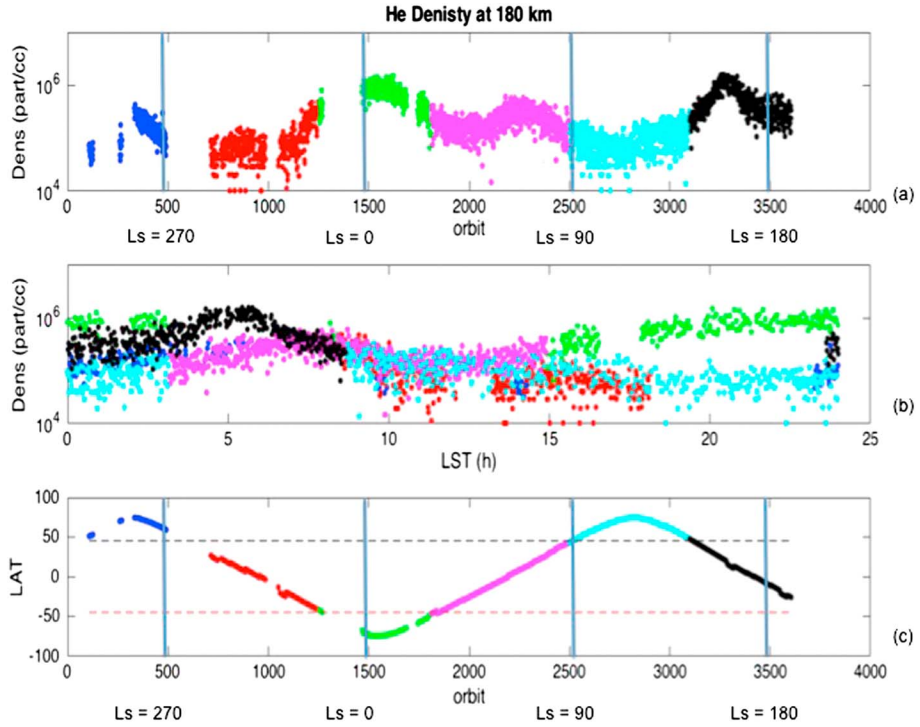

Figure 3. Vertical lines mark Ls = 0°, 90°, 180°, and 270° with the colors set by latitudes measured as illustrated in Figure 3c. (a) He density at 180 km plotted over time (orbit number). Gaps in the data are due to spacecraft entering safe mode and solar conjunction. (b) He density versus LST at 200 km. Peak at LST = 2–5 h with a second peak around LST = 20 h. The split in the data around LST = 20 h is due to latitude differences. (c) latitude versus orbit number to illustrate the track of the orbit and track Ls. Each region is broken up along 45°N and 45°S indicated by the black and red lines in Figure 3c.

the northern polar region was from Ls = 88–150, during northern summer (Figure 1c). While the first pass was during commissioning, and there were several data gaps due to spacecraft safing events early in the mission, the second pass was complete, and thus, coverage of the north polar region is adequate to determine a He Bulge on the nightside with a winter enhancement. MAVEN sampled the southern polar region around Ls = 331–50 during equinox. The coverage in the southern polar region did show a peak during the nightside; however, there was inadequate coverage on the dayside during this portion of the campaign to show a significant contrast to the nightside southern polar region, or to make any seasonal conclusions in the south. The southern polar region did show a substantial nightside enhancement compared with dayside measurements in agreement with a diurnal driver. Due to Mars' large eccentricity, it would not be surprising to see different characteristic He signatures in the northern and southern polar regions. It is possible with a longer and more pronounced southern winter, the He bulge could accumulate more in southern winter. More data would need to be obtained to support this theory. It is our recommendation that while these data do support a strong He bulge in the southern polar region driven by diurnal effects, and the He density does appear to be higher than the northern polar region, more data in the southern region are needed to confirm our hypothesis.

A peak in He abundances was also observed on the nightside in the equatorial region. The remainder of the data taken between ±45°N and 45°S supports the strong diurnal effects with a secondary seasonal driver. This bulge was most obvious, however, closest to the southern bulge near equinox, when the bulge is likely to be shifting in intensity from one pole to the other. Figure 3 takes a slice of the He density at a constant altitude of 200 km and plots values along time (orbit #), LST, and Ls. Vertical lines are included to mark where Ls 0, 90, 180, and 270 occur along the orbit number track for reference. By taking a slice at constant altitude, it is possible to examine the variations in the atmosphere eliminating any altitude effects due to the He large scale height. Figure 4 shows the strong diurnal effect leading to the primary He density peaks at LST ~2–5 h.

In order to better understand the diurnal effects, we examined the changes in the CO_2 densities as well as how they are related to the He densities with respect to LST. The CO_2 atmosphere fluctuates primarily with the

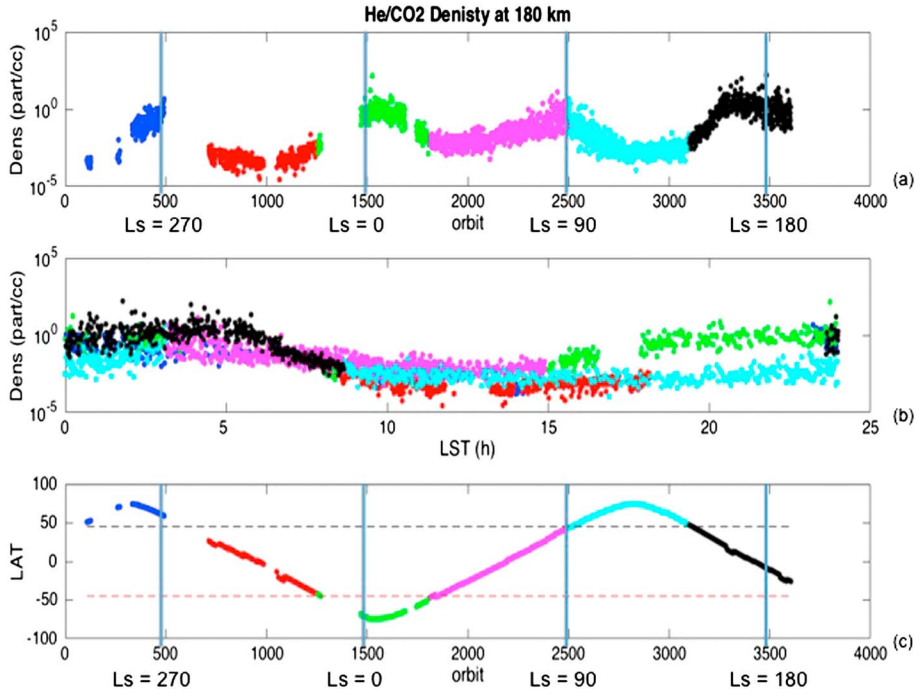

Figure 4. He/CO_2 ratio over time: Vertical lines at Ls = 0, 90, 180, and 270. Colors are consistent in each panel to allow tracking. (a) He/CO_2 ratio versus orbit. As CO_2 increases, He decreases, and vice versa. The ratio is highest for highest He. (b) He/CO_2 ratio versus LST. The ratio peaks for LST = 2–5 h consistent with highest He densities. CO_2 is falling off as He is increasing in agreement with model results. This demonstrates a He peak near dawn ~2–5 h with a secondary peak around 20 h. This indicates much higher He densities and He/CO_2 ratio at dawn indicating a diurnal with a possible seasonal effect. (c) LAT versus orbit number to illustrate the track of the orbit and track Ls.

atmospheric neutral temperature; i.e., as the temperatures cool (especially on the nightside), the atmospheric column contracts, and the CO_2 thermospheric densities decrease at a constant altitude. Conversely, as temperatures warm (generally on the dayside), the atmospheric expands and thermospheric CO_2 densities increase. This is opposite to the He density variation of the upper atmosphere (above the homopause). As He is a light species (with a correspondingly large scale height), its horizontal distribution may be driven by local vertical advection resulting from the thermospheric circulation pattern similar to Earth [e.g., *Liu et al.*, 2014], whereas, the He, due to its very high scale height and escape rate, is not significantly affected by the atmospheric heating and cooling but is more affected by the winds. He is preferentially enhanced on the nightside where it collects in those regions where the horizontal winds converge and vertical downwelling is strongest. This combination of He and CO_2 variations yields a useful diagnostic that clearly isolates the He bulges; i.e., the ratio of He/CO_2 reveals "hot spots" indicative of these bulges. Figure 4 tracks the ratio of He/CO_2, at 200 km in order to demonstrate this strong diurnal dependence with seasonal enhancement. Similarly to Figure 3, each region (northern, southern, and equatorial) is color coded in order to make the ratio easy to track in terms of LST and past LS and orbit number. Figure 4a compares to orbit number, (b) LST, and (c) orbit versus LAT; vertical lines mark the Ls = 0, 90, 180, and 270 in the same way as Figure 3. This again reveals the same peaks seen before near LST 2–5. When comparing the two northern regions (blue and cyan), this ratio has two distinct behaviors considering both can be comparable in terms of similar LST. This indicates that in the northern region there was a seasonal enhancement to the bulge. The much higher peaks around Ls = 90 and 180 are most likely due to the dominance of a diurnal effect with a slight influence from a seasonal effect. More data with better coverage will help to determine the effect better.

One possible explanation for a larger southern polar He bulge at equinox versus the smaller northern polar He bulge at winter both occurring at night, could be an instrumental effect. Early in the mission NGIMS was originally set to operate with the filaments on high emission in order to maximize neutral gas detection. In this mode, we discovered that the background on all mass channels ended up being much higher than anticipated, and backscattering effects from Ar and CO_2 near periapsis affecting lower mass channels was

more significant than anticipated. Along with some other settings to mitigate the background, we elected to set the filaments on their lower setting starting on 15 February2015, just before the first deep dip pass. While this instrumentation effect was significant to the major species (CO_2, Ar, N_2, O, O_2, and CO), and the NGIMS team strongly recommends using data from 14 February 2015 onward, these initial settings had little impact on the detection of He. The impact on the CO_2 and Ar detection was significant, and as a major component of the atmosphere and a major element in Figure 3, it will affect the early data from the northern polar region only. No neutral data are available for any species including the lighter He from 29 December 2014 to 14 February 2015 due to this contamination issue. For this study we only used data with good pointing, and adequate signal above the noise for all species. In Figures 3 and 4 it affects blue dots up to the third large gap in data. Thus, the first winter densities in the northern hemisphere may have a slightly higher background than all other densities, and the corrections for background may have abnormally lowered the densities for this small segment of data. Though He generally has a background near 0, CO_2 has a very high background and this was a much larger effect on the major species.

1.2. Methods: M-GITM

The Mars Global Ionosphere-Thermosphere Model (M-GITM) is a model framework combining the terrestrial GITM framework [*Ridley et al*., 2006] with Mars fundamental physical parameters, ion-neutral chemistry, and key radiative processes in order to capture the basic observed features of the thermal, compositional, and dynamical structure of the Mars atmosphere from the ground to ~250 km [*Bougher et al*., 2015b]. M-GITM simulates the conditions of the Martian atmosphere all the way to the surface, with an emphasis on upper atmosphere processes. Simulated three-dimensional upper atmosphere (80–250 km) fields include neutral temperatures, densities (CO_2, CO, O, N2, O_2, He, etc), winds (zonal, meridional, and vertical), and photochemical ions (O+, O2+, CO_2+, N_2+, and NO+). Simulations spanning the full range of applications of the current M-GITM code, including 12 model runs spanning various solar cycle and seasonal conditions, have been completed and the results are described in a comprehensive initial paper [*Bougher et al*., 2015b].

The M-GITM upper atmosphere physics, chemistry, and formulations are the most complete, and therefore, MAVEN data-model comparisons thus far have largely focused on this region above ~100 km. At this point, M-GITM simulations have been compared with NGIMS measurements obtained during its first year of operations during four Deep Dip campaigns [*Bougher et al*., 2015a, 2015b]. In particular, Deep Dip 2 (DD2) temperatures and key neutral densities have been compared with corresponding M-GITM fields extracted along DD2 orbit trajectories on the dayside near the equator [*Bougher et al*., 2015a]; a good match of key neutral densities and temperatures is revealed for nightside measurements.

The M-GITM model suggests that the He bulge will be strongest around the poles and weaker in the equatorial region. Slices of the global model at 200 km are taken at various seasons (Ls = 0, 90, 180, and 270) as shown in Figure 5. These panels reveal a stronger bulge in the northern polar region (Ls = 270), at midlatitudes (Ls = 0 and 180) and around the southern polar region (Ls = 90) at LST = 2–5 h. These are global results, and when coverage from the MAVEN mission becomes more global, detailed He comparisons between NGIMS data and the model will be possible. Figure 6 compares LAT versus LST (a) of He density for the entire year; conversely CO_2 density for the entire year LAT versus LST (b) all four panels at 200 km. For certain configurations this compares well with the model, for others, more data are needed.

While comparison between Figures 5 and 6 is difficult because coverage from MAVEN is still very incomplete, it is possible to make some comparisons. Figure 6 shows a strong He bulge at LST = 2–5 h at the northern and southern polar regions. Additionally, between LST = 15 h and LST = 20 h is a secondary peak in the southern hemisphere. This secondary peak corresponds with Ls = 90 and Ls = 180 from Figure 3 indicating that these occurred during equinox. While direct match between data and model is difficult due to coverage gaps, it is possible to observe nightside He accumulations and enhancement of the He bulge at the poles versus over the equatorial region as predicted by the model.

2. Discussion

With the MAVEN NGIMS measurements He bulges have now been discovered in the thermospheres of Earth, Venus, and Mars [e.g., *Levine et al*., 1974; *Reber and Hays*, 1973; *Niemann et al*., 1980; *Kockarts*, 1973]. The seasonal responses of these bulges are most evident at Earth and Mars. At Earth, the He bulge has been found to be

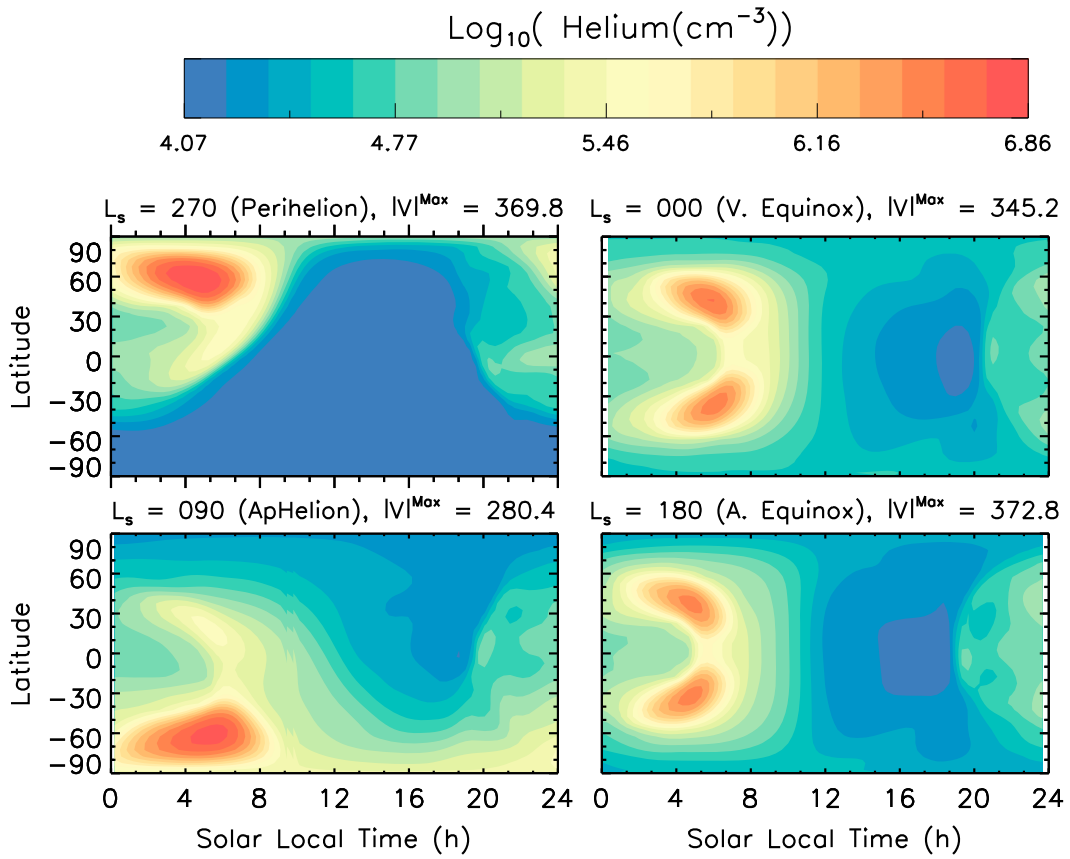

Figure 5. M-GITM results at a constant altitude of 200 km shows LAT versus LST. Each panel represents a different slice at a different Ls; Ls = 270, Ls = 0, Ls = 90, and Ls = 180. In each panel the He bulge occurs near Ls = 2–5 and shifts between the northern and southern poles with the seasons. As these are global model results, it has complete coverage beyond MAVEN data coverage. Dark blue here is low counts as opposed to missing data.

strongly seasonally dependent [*Liu et al.*, 2014; *Sutton et al.*, 2015]. It is highest at the poles in winter and lowest at summer. Terrestrial bulges have an enhancement feature associated with LST = 4 at 400 km. Simulations from the three-dimensional Thermosphere Ionosphere Electrodynamic GCM (TIEGCM) have shown that the large difference between the summer and winter He bulge is mostly dependent on local vertical advection and molecular diffusion [*Liu et al.*, 2014; *Sutton et al.*, 2015]. Early modeling efforts to describe the He bulge varied the eddy diffusion coefficients [*Krasnopolsky et al.*, 1994; *Kasprzak et al.*, 1993]. However, more recent modeling efforts found that vertical advection (connected to the interhemispheric circulation) has a stronger effect [*Liu et al.*, 2014]. Specifically, seasonally varying horizontal winds indirectly contribute to the winter He bulge formation, as their divergence drives local vertical winds in order to satisfy mass continuity in the thermospheric general circulation. As a light inert gas, Earth thermospheric He distributions are very sensitive to local vertical advection, especially in regions of convergence and downwelling of the thermospheric circulation (e.g., winter polar regions) [*Cageao and Kerr*, 1984]. This makes He a sensitive tracer of the seasonally varying circulation pattern (and associated local vertical advection) for Earth.

The diurnal and seasonal effects on the He bulge for Mars indicate that there is possibly upward advection in the dayside summer hemisphere and downward advection in addition to the thermospheric circulation in the winter nightside creating the polar He bulges. As shown above for Mars, He densities are strongly enhanced for the nightside versus the dayside, revealing bulges at polar latitudes in and midlatitudes (equinox) during early morning (LST = 2–5). Additionally, the two data sets from the northern polar region, (winter and summer) show approximately a factor of 2 difference in abundance between the nightside bulges indicating a seasonal enhancement in the northern polar region during the winter. As can be seen in Figure 5, the model demonstrates that the diurnal effects in the polar regions at their peak, "winter"(Ls 270 or Ls 90) have an order of magnitude difference between night and dayside in agreement with the NGIMS data.

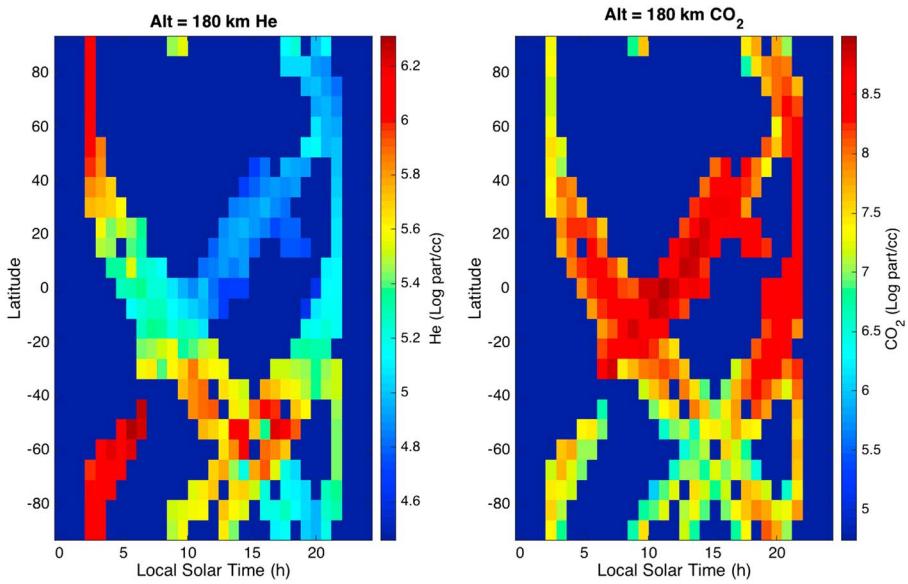

Figure 6. Constant altitude latitude versus LST: LAT versus LST He density, and CO_2 density. He is highest at high latitudes, LST = 2–5 h. Since this is for the entire year and complete data set, there are some similarities between the data set and the M-GITM model results (Note that dark blue indicates no data taken yet by MAVEN not just low counts and teal or light blue indicates lowest measured data).

At the lowest points, "summer," the diurnal effects in the polar regions are much smaller, half and order magnitude to and order of magnitude. At the equinox, the diurnal bulges are reduced by half in both polar regions. It is this combination that indicates not only that there should be a diurnal but also a seasonal effect according to the model. NGIMS data, thus far, have found a smaller seasonal effect than the model predicts, which is likely largely due to lower coverage than needed to obtain the complete global picture from the M-GITM model.

Once again, it is likely that the global thermospheric circulation is primarily responsible with a secondary effect coming from vertical advective winds, consistent with dayside divergence (upwelling) and nightside convergence (downwelling) of the global wind pattern. Local nightside vertical advection produces a He bulge at the convergence (maximum downwelling) point of the circulation.

Since Mars indeed has seasons, the changing seasonal thermospheric circulation pattern is simulated by M-GITM [e.g., *Bougher et al.*, 2015; *Roble et al.*, 1988], providing divergence on the dayside at midafternoon subsolar latitudes, and convergence on the nightside. This nightside convergence point moves with season, resulting in polar enhancements of He in the winter hemisphere during the solstices, and midlatitude enhancements of He densities during equinoxes. With Mars' larger eccentricity, the southern winter will be more pronounced than northern winter. This elongation of the southern winter season could also drag the He bulge south longer than the northern bulge delaying the transport north after southern winter. It is this delay that could help explain the much larger He bulge in the southern hemisphere at Ls = 0 on the nightside over the He bulge in the northern hemisphere near Ls = 270 at the nightside. More modeling and measurement of Mars winds will continue to help explain these phenomena.

MAVEN NGIMS is in the process of measuring the upper atmosphere winds [*Bougher et al.*, 2016]. While direct measurements of the atmospheric winds are still pending, our results indicate that seasonally varying global winds yield seasonally varying downwelling winds (and vertical advection) that control the location and magnitude of the He bulge.

Conversely, Venus has no seasons, so this pattern is basically composed of a subsolar to antisolar circulation (stable), with a highly variable superimposed retrograde zonal (RSZ) component flow [e.g., *Bougher et al.*, 1997; *Keating and Bougher*, 1987]. Resulting Venusian He densities are higher on the nightside (LST 2–5) than during the day near the equator, exactly opposite to the behavior for CO_2 densities [*von Zahn et al.*, 1983; *Niemann et al.*, 1980; *Hartle et al.*, 1996]. The mechanism for He bulge formation may be similar to Earth

and Mars, with enhanced vertical advection at the convergence point (maximum downweling winds) at the location of the bulge maximum. It is remarkable that the LST = 2–5 region for convergence in all Mars seasons is similar to that Venus. This similarity between Mars and Venus He bulge will help to explain the strong southern polar bulge occurring during equinox, which is unrelated to the seasonal effects noted at the northern polar region.

3. Summary

MAVEN NGIMS neutral measurements of He and CO_2 in the upper atmosphere of Mars revealed a peak in the He densities for LST = 2–5 h with a secondary peak around LST = 22–24 h. While He densities maximize on the nightside with an enhancement due to latitudinal (i.e., polar) and seasonal effects, NGIMS data also demonstrated that CO_2 densities were decreasing (dayside to nightside), similar to trends found at Venus. He bulges have been detected on Venus, Earth, and now confirmed on Mars [*Krasnopolsky and Gladstone*, 1996, 2005; *Krasnolpolsky et al*., 1994, 1993]. The presence of a seasonal and diurnally dependent He bulge in the upper atmosphere is an indicator of strong local vertical advection (downwelling) in the nightside (often winter polar) thermosphere associated with the variable interhemispheric circulation pattern. He, being the lighter species, is driven primarily by the thermospheric circulation (and not the temperature distribution), inversely to that of the heavier elements like CO_2 and Ar. This is why there are larger He abundances on the nightside, especially at the polar regions than at the equatorial and dayside locations where CO_2 abundances are higher and He is lower.

Acknowledgments
Special acknowledgments to the MAVEN NGIMS team at NASA Goddard SFC, and the MAVEN operations team at LASP and Lockheed Martin in Colorado. All data are archived in the Planetary Atmospheres Node of the Planetary Data System (http://pds.nasa.gov). Data through 15 August 2016 are available on the Planetary Data System (PDS4) (e.g., mvn_ngi_l2_csn-abund-14015_20141018T100458_v06_r02.csv *mvn_ngi_l2_cso-abund-20708_20160804T173834_v06_r02.csv*). These data are available upon request. The MAVEN mission has been funded by NASA through the Mars Exploration Program.

References

Bell, J. M., S. W. Bougher, P. M. Mahaffy, and M. K. Elrod (2015), Simulating helium abundances in the Martian upper atmosphere using 1-D and 3-D models*, AAS DPS meeting #47 id 419.21*.
Bougher, S. W., and R. Roble (2003), Helium as a tracer of terrestrial planet upper atmosphere dynamics: Predictions for Mars, *AGU abstract*
Bougher, S. W., R. E. Dickenson, E. C. Ridley, and R. G. Roble (1986), Venus mesosphere and thermosphere: III. Three-dimensional general circulation with coupled dynamics and composition, *Icarus*, *73*, 545–573, doi:10.1016/0019-1035(88)90064-4.
Bougher, S. W., R. G. Roble, E. C. Ridley, and R. E. Dickinson (1990), The Mars thermosphere .2. General-circulation with coupled dynamics and composition, *J. Geophys. Res.*, *95*, 14,811–14,827, doi:10.1029/Jb095ib09p14811.
Bougher, S. W., M. J. Alexander, and H. G. Mayr (1997), Chapter 9: Upper atmospheric dynamics: Global circulation and gravity waves, in *Venus II: Geology, Geophysics, Atmosphere, and Solar Wind Environment*, edited by S. W. Bougher, D. M. Hunten, and R. J. Phillips, pp. 259–292, Univ. of Arizona Press, Tucson.
Bougher, S. W., et al. (2015a), Early MAVEN dip deep campaign reveals thermosphere and ionosphere variability, *Science*, *350*, 1–7, doi:10.1126/science.aad0459.
Bougher, S. W., J. M. Bell, K. Olsen, K. Roeten, P. R. Mahaffy, M. Elrod, M. Benna, and B. M. Jakosky (2015b) Variability of Mars thermospheric neutral structure from MAVEN deep dip observations: NGIMS comparisons with global models, *EOS*, 2015 Supplement(74805)
Bougher, S. W., K. J. Roeten, K. G. Olsen, P. R. Mahaffy, M. Benna, M. K. Elrod, J. M. Bell, and B. M. Jakosky (2016), Variability of the thermospheric wind structure of Mars: MAVEN NGIMS measurements and corresponding global model simulations, *AGU Fall Meeting* P13D–05.
Cageao, R. P., and R. B. Kerr (1984), Global distribution of helium in the upper atmosphere during solar minimum, *Planet. Space Sci.*, *32*(12), 1523–1529, doi:10.1016/0032-0633(84)90019-9.
Hartle, R. E., T. M. Donahue, J. M. Grebowsky, and H. G. Mayr (1996), Hydrogen and deuterium in the thermosphere of Venus: Solar cycle variations and escape, *J. Geophys. Res.*, *101*, 4525–4538, doi:10.1029/95JE02978.
Jakosky, B. M., et al. (2014), The Mars Atmosphere and Volatile Evolution (MAVEN) mission, *Space Sci. Rev.*, doi:10.1007/s11214-015-0139-x.
Kasprzak, W. T. (1969), Evidence for a helium flux in the lower thermosphere, *J. Geophys. Res.*, *74*, 894–896, doi:10.1029/JA074i003p00894.
Kasprzak, W. T., H. B. Neiman, and A. E. Hedin (1993), Neutral composition measurements by the pioneer Venus neutral mass spectrometer during orbiter re-entry, *Geophys. Res. Lett.*, *20*, 2747–2750, doi:10.1029/93GL02241.
Keating, G. M., and S. Bougher (1987), Neutral upper atmospheres of Venus and Mars, *Adv. Space Res.*, *7*(12), 1257–1271, doi:10.1016/0273-1177(87)90202-X.
Kockarts, G. (1973), Helium in the terrestrial atmosphere, *Space Sci. Rev.*, *14*, 723, doi:10.1007/BF00224775.
Krasnopolsky, V. A. (2002), Mars' upper atmosphere and ionosphere at low, medium, and high solar activities: Implications for evolution of water, *J. Geophys. Res.*, *107*(E12), 5128, doi:10.1029/2001JE001809.
Krasnopolsky, V. A., and G. R. Gladstone (1996), Helium on Mars: EUVE and PHOBOS data and implications for Mars' evolution, *J. Geophys. Res.*, *101*, 15,765–15,772, doi:10.1029/96JA01080.
Krasnopolsky, V. A., and G. R. Gladstone (2005), Helium on Mars and Venus: EUVE observations and modeling, *Icarus*, *176*, 395–407, doi:10.1029/93GL02241.
Krasnopolsky, V. A., S. Chakrabarti, and G. R. Gladstone (1993), Helium in the Martian atmosphere, *J. Geophys. Res.*, *98*, 15,061–15,068, doi:10.1029/93JE00534.
Krasnopolsky, V. A., S. Bowyer, S. Chakrabarti, G. R. Gladstone, and J. S. McDonald (1994), First measurement of helium on Mars: Implications for the problem of radiogenic gases on the terrestrial planets, *Icarus*, *109*, 337–351, doi:10.1006/icar.1994.1098.
Levine, J. S., G. M. Keating, and E. J. Prior (1974), Helium in the Martian atmosphere: Thermal loss considerations, *Planet. Space Sci.*, *22*(3), 500–503, doi:10.1016/0032-0633(74)90082-8.
Liu, X., W. Wang, J. P. Thayer, A. Burns, E. Sutton, S. C. Solomon, L. Qian, and G. Lucas (2014), The winter helium bulge revisited, *Geophys. Res. Lett.*, *41*, 6603–6609, doi:10.1002/2014GL061471.

Mahaffy, P. R., et al. (2014), The Neutral gas and ion mass spectrometer on the Mars atmosphere and volatile evolution mission, *Space Sci. Rev.*, *195*(1), 49–73, doi:10.1007/s11214-014-0091-1.

Mahaffy, P. R., M. Benna, M. Elrod, R. V. Yelle, S. W. Bougher, S. W. Stone, and B. M. Jakosky (2015), Structure and composition of the neutral upper atmosphere of Mars from the MAVEN NGIMS investigation, *Geophys. Res. Lett.*, *42*, 8951–8957, doi:10.1002/2015GL065329.

Neir, A. O., and M. B. McElroy (1977), Composition and structure of Mars' upper atmosphere—Results from the neutral mass spectrometers on Viking 1 and 2, *J. Geophys. Res.*, *82*, 4341–4349, doi:10.1029/JS082i028p04341.

Niemann, H. B., W. T. Kasprzak, A. E. Hedin, D. M. Hunten, and N. W. Spencer (1980), Mass spectrometric measurements of the neutral gas composition of the thermosphere and exosphere of Venus, *J. Geophys. Res.*, *85*, 7817–7827, doi:10.1029/JA085iA13p07817.

Reber, C. A., and P. B. Hays (1973), Thermospheric wind effects on the distribution of helium and argon in the Earth's upper atmosphere, *J. Geophys. Res.*, *78*, 2977–2991, doi:10.1029/JA078i016p02977.

Ridley, A., Y. Deng, and G. Toth (2006), The global ionosphere-thermosphere model, *J. Atmos. Sol. Terr. Phys.*, *68*, 839, doi:10.1016/j.jastp.2006.01.008.

Roble, R. G., E. C. Ridley, A. D. Richmond, and R. E. Dickinson (1988), A coupled thermosphere/ionosphere general circulation model, *Geophys. Res. Lett.*, *15*, 1325–1328, doi:10.1029/GL015i012p01325.

Sutton, E. K., J. P. Thayer, W. Wang, S. C. Solomon, X. Liu, and B. T. Foster (2015), A self-consistent model of helium in the thermosphere, *J. Geophys. Res. Space Physics*, *120*, 6884–6900, doi:10.1002/2015JA021223.

Von Zahn, U., S. Kumar, H. Niemann, and R. Prinn (1983), Chapter 13: Composition of the Venus Atmosphere, in *Venus Book*, edited by D. M. Hunten et al., pp. 297–430, Univ. of Arizona Press, Tucson.